Supporting Information

In-Situ **Formed Bimetallic Carbide Ni_6Mo_6C Nanodots and $NiMoO_x$ Nanosheet Arrays Hybrids Anchored on Carbon Cloth: Efficient and Flexible Self-supported Catalysts for Hydrogen Evolution**

*Xiaozhong Zheng, Yuzhuo Chen, Xiaobing Bao, Shanjun Mao, Ruxue Fan, and Yong Wang**

Advanced Materials and Catalysis Group, Institute of Catalysis, Department of Chemistry, 310028, Zhejiang University, Hangzhou, P. R. China.

E-mail: chemwy@zju.edu.cn

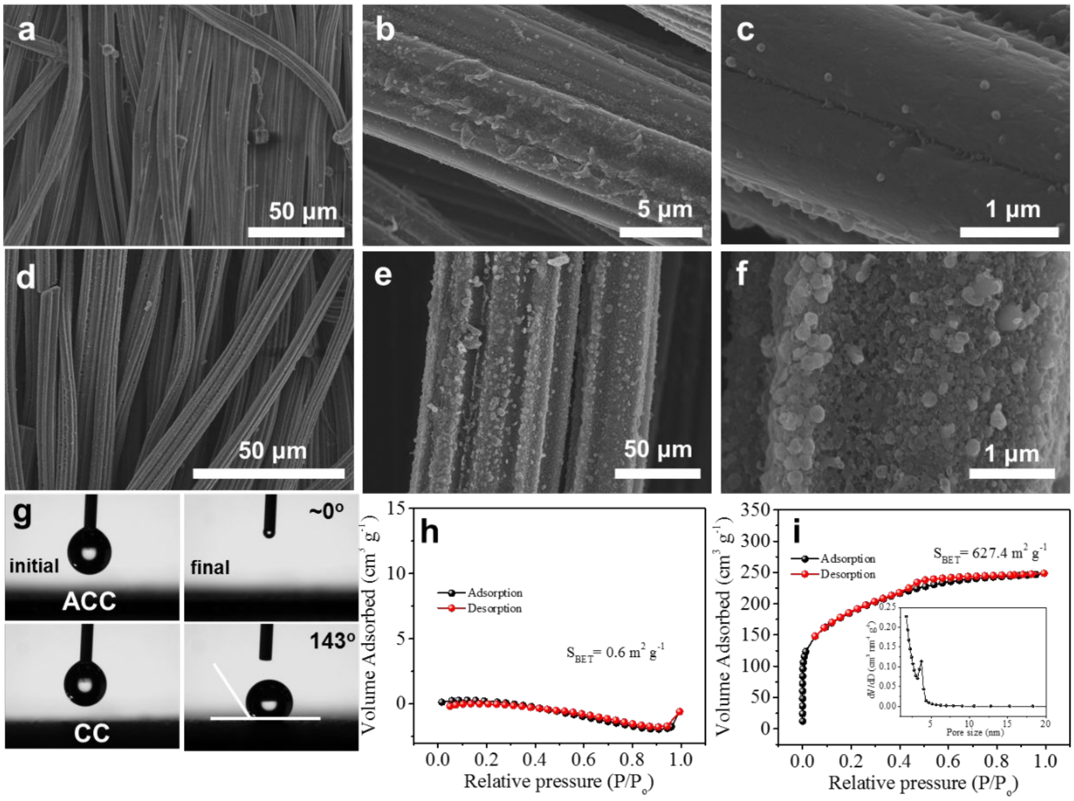

Figure S1. (a), (b), (c) FE-SEM images of the carbon cloth (CC); (d), (e), (f) FE-SEM images of the actived carbon cloth (ACC); (g) Contact angle test of CC and ACC; (h), (j) Nitrogen adsorption-desorption isotherms of CC and ACC, respectively.

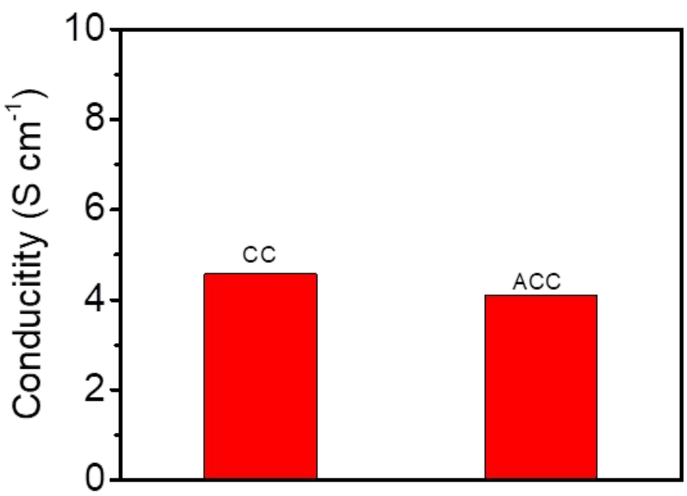

Figure S2. Conductivity of carbon cloth (CC) activated carbon cloth (ACC).

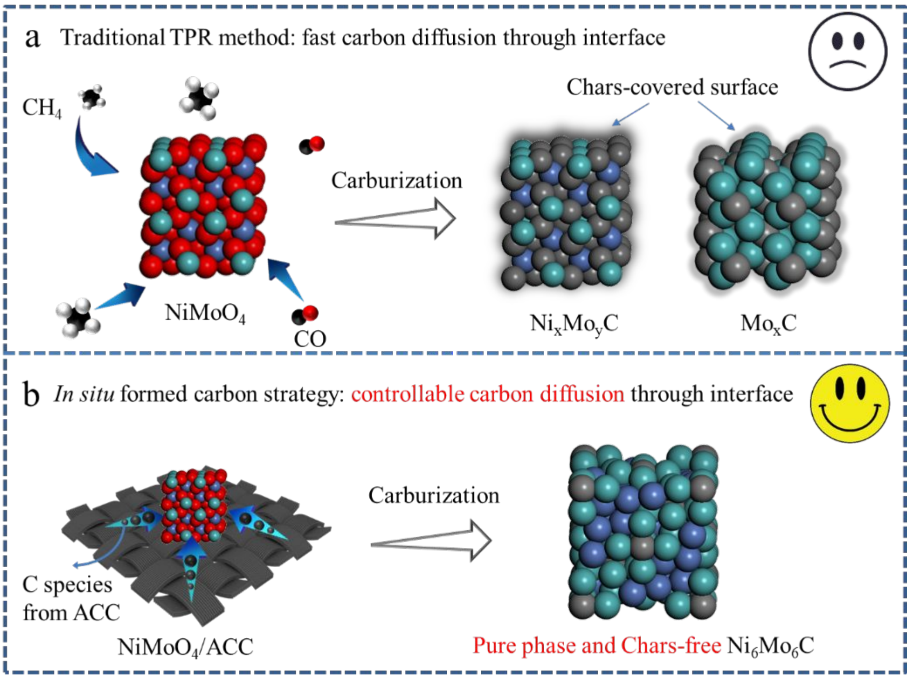

Figure S3. Schematic diagram of traditional TPR method (a) and *in situ* formed carbon strategy (b) for constructing metal carbides.

Figure S4. Digital photo of $NiMoO_4$/ACC and $Ni_6Mo_6C/NiMoO_x$/ACC.

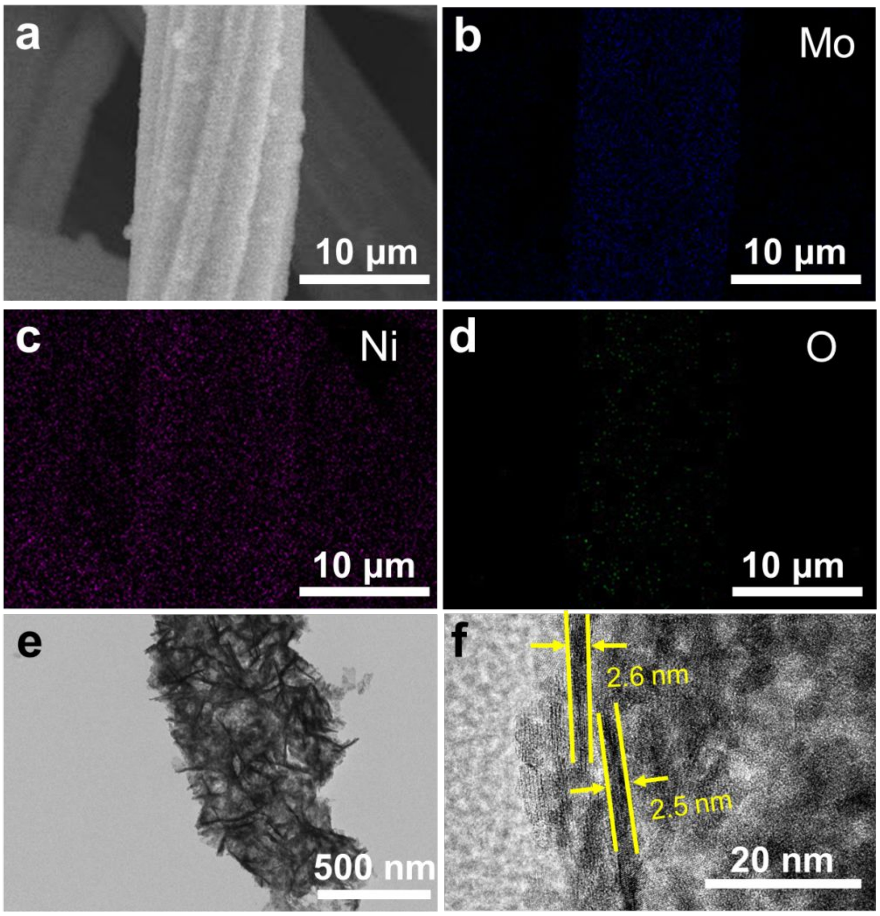

Figure S5. (a) SEM image, (b-d) corresponding elemental mapping images and TEM images (e) and HRTEM (f) of $NiMoO_4$/ACC.

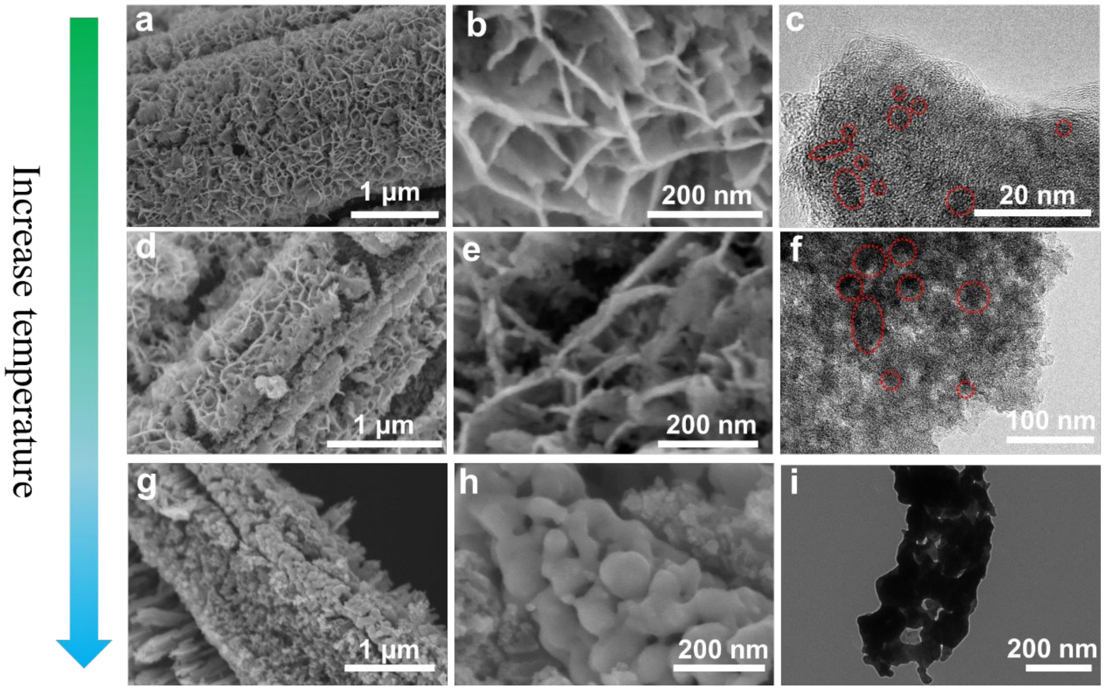

Figure S6. SEM images and TEM image of $Ni_6Mo_6C/NiMoOx$-300 (a, b, c), $Ni_6Mo_6C/NiMoO_x$-500 (d, e, f) and Ni_6Mo_6C/Mo_2C-600 (g, h, i).

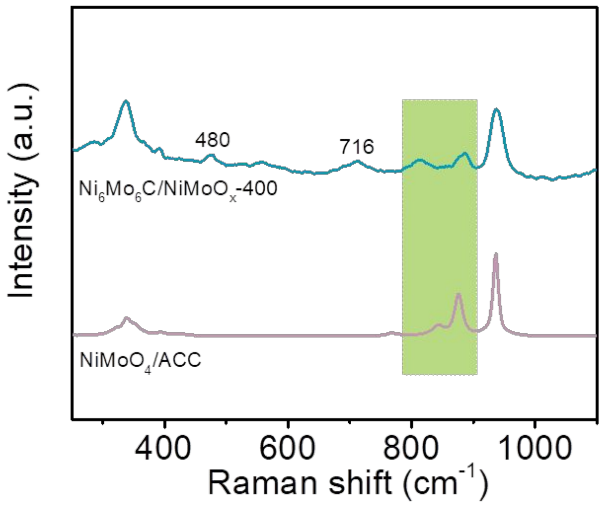

Figure S7. (a) EPR spectra and (b) Raman spectra of $NiMoO_4$/ACC and $Ni_6Mo_6C/NiMoO_x$-400.

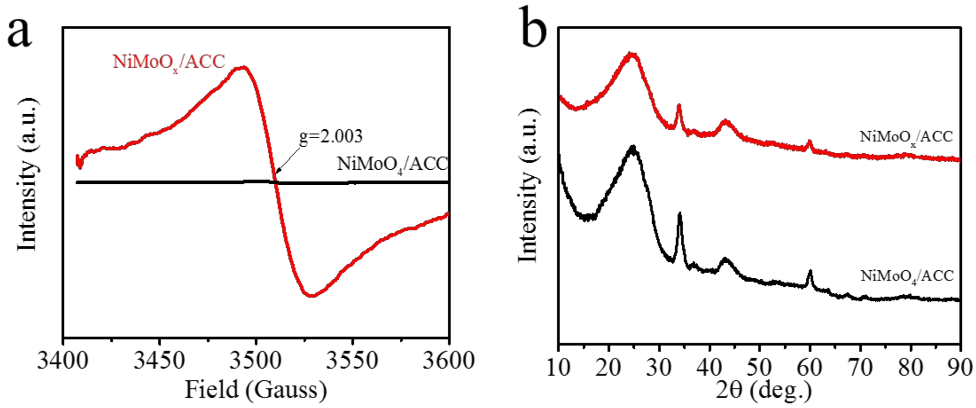

Figure S8. EPR spectra (a) and XRD patterns (b) of $NiMoO_4$/ACC and $NiMoO_x$/ACC.

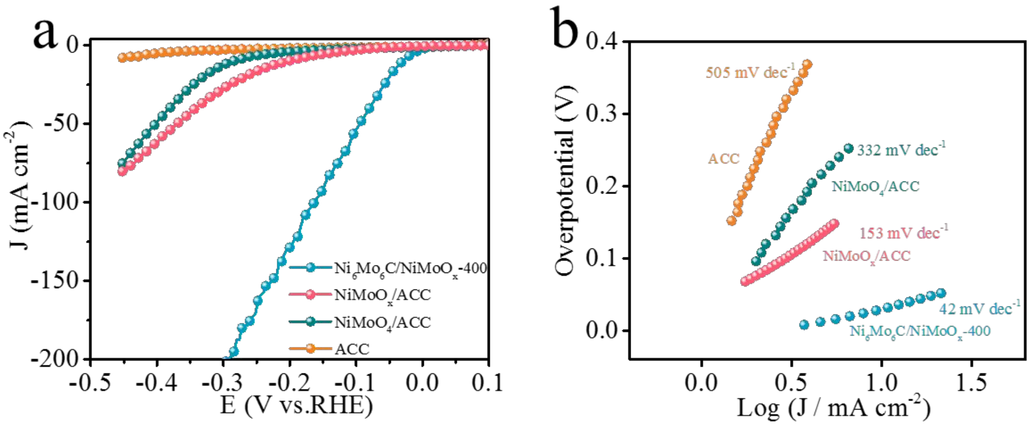

Figure S9. (a) HER polarization curves and (b) Tafel slope plots of $Ni_6Mo_6C/NiMoO_x$-400, $NiMoO_x$/ACC, $NiMoO_4$/ACC precursor and carbon substrate ACC.

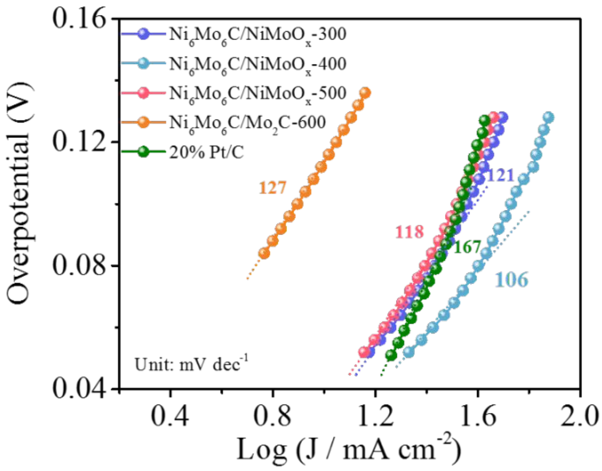

Figure S10. Tafel plots obtained from the polarization curves at a large overpotential range (>50 mV) in 1.0 M KOH electrolyte.

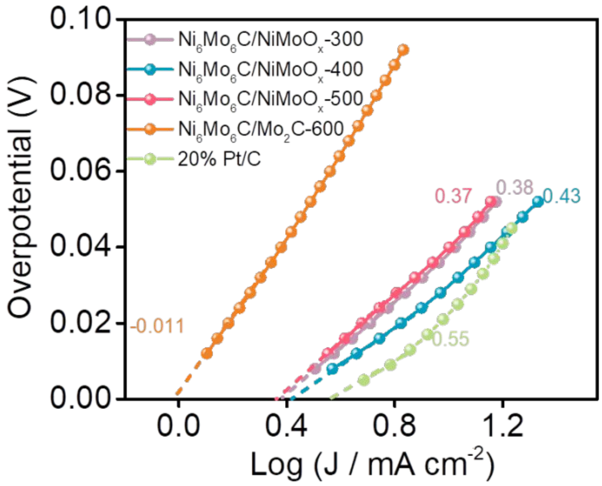

Figure S11. Exchange current density of various catalysts through extrapolation of Tafel plots in low overpotential region.

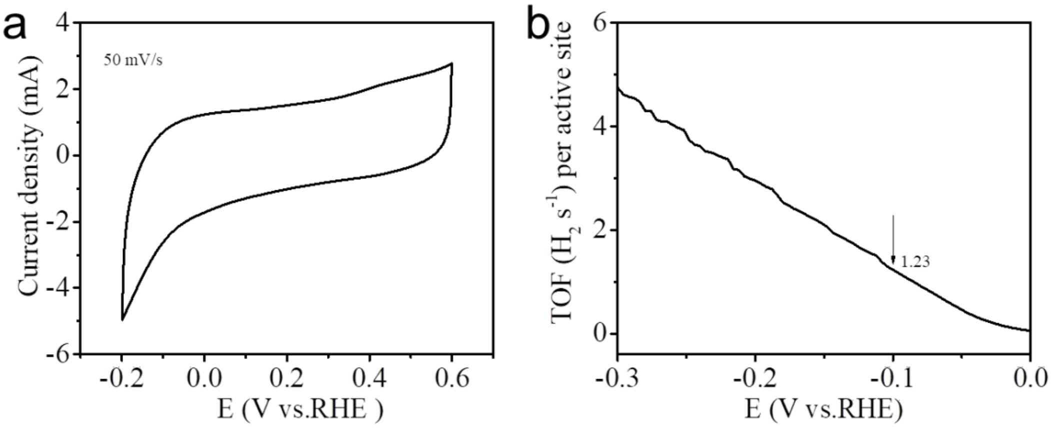

Figure S12. (a) CV of $Ni_6Mo_6C/NiMoO_x$-400 in 1 M PBS (pH =7) with a scan rate of 50 mV s^{-1}. (b) The calculated turnover frequency curve of $Ni_6Mo_6C/NiMoO_x$-400 catalyst for HER.

The TOF of $Ni_6Mo_6C/NiMoO_x$-400 for HER was calculated based on a electrochemical CV method. Figure S9a shows CV curve in the region of -0.2 to 0.6 V vs. RHE for $Ni_6Mo_6C/NiMoO_x$-400 in 1 M phosphate buffer solution (PBS, pH = 7). The integrated charge over the whole potential range should be proportional to the total number of active sites. Assuming a one-electron process for both reduction and oxidation process, the upper limit of active sites could be calculated. Figure S9b shows the polarization curves in 1 M KOH, normalized by the active sites and expressed in terms of TOF. The turnover frequency (TOF) value at overpotential of 100 mV is 1.23 s^{-1} in alkaline media, which is larger than those for reported Mo_2C-based materials and so on. (the TOF values of these catalysts at 100 mV usually below 1.0 s^{-1})

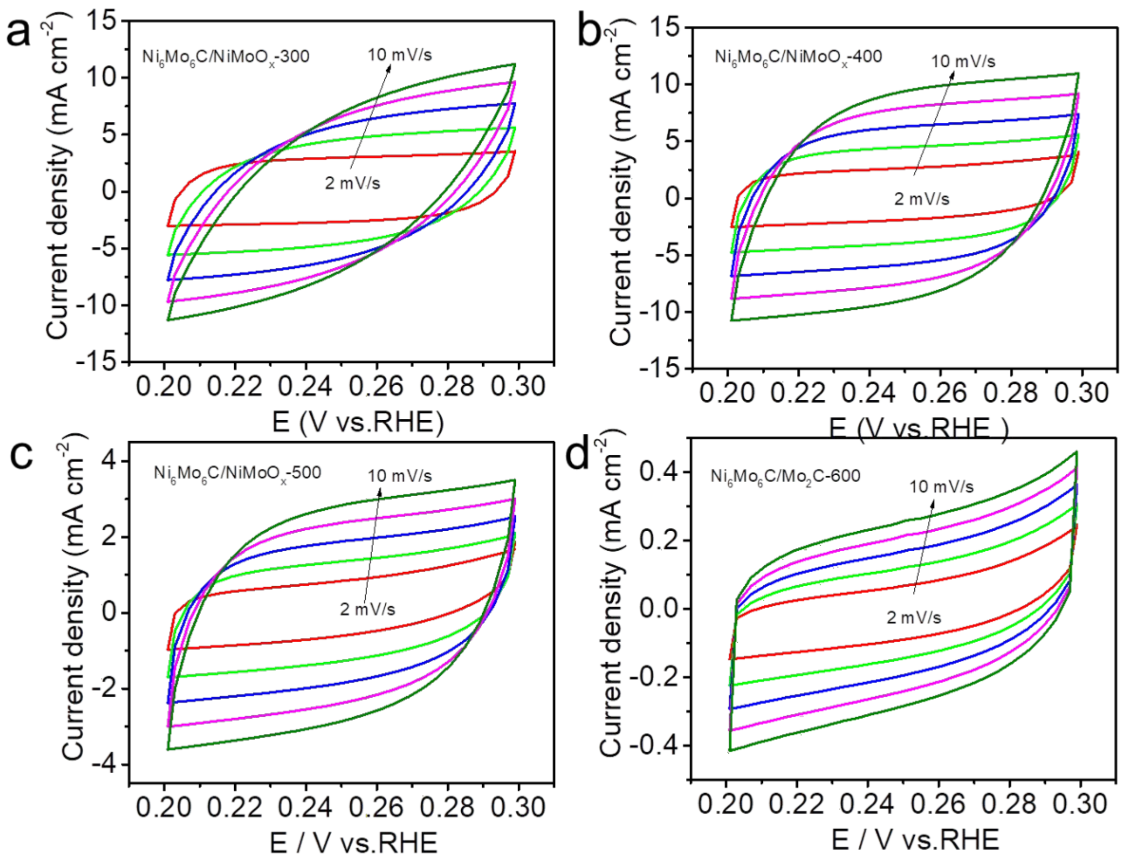

Figure S13. Cyclic voltammetry of (a-d) $Ni_6Mo_6C/NiMoO_x$-T, respectively, the arrows represent the increased scan rate from 2 mV/s to 10 mV/s.

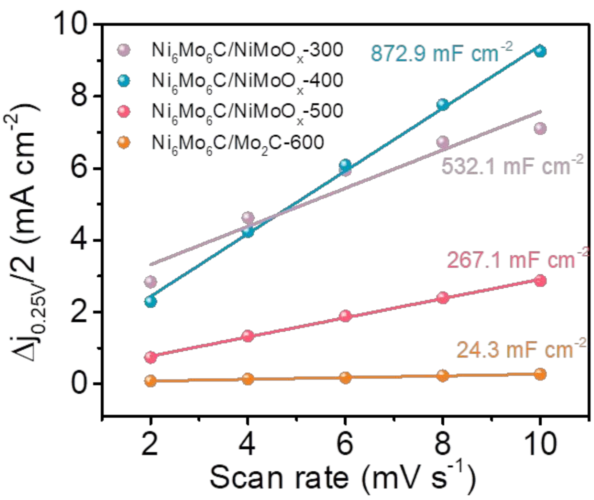

Figure S14. The capacitive currents at 0.25 V vs. RHE against scan rate fitted to a linear regression enables the estimation of C_{dl}, where the slope are C_{dl} of $Ni_6Mo_6C/NiMoO_x$-T.

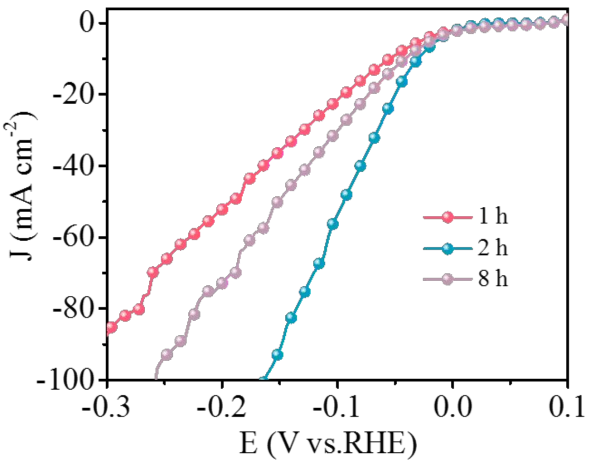

Figure S15. The HER polarization curves of $Ni_6Mo_6C/NiMoOx$-400 with different calcination time.

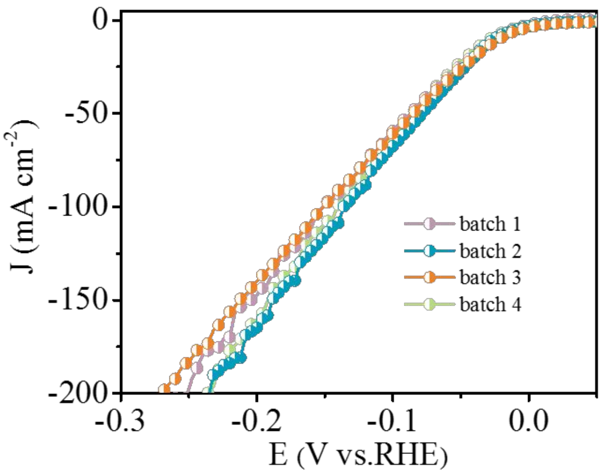

Figure S16. The polarization curves for different batches of $Ni_6Mo_6C/NiMoO_x$-400 under the same electrochemical conditions; the data of batch 1 is presented in Figure 3a.

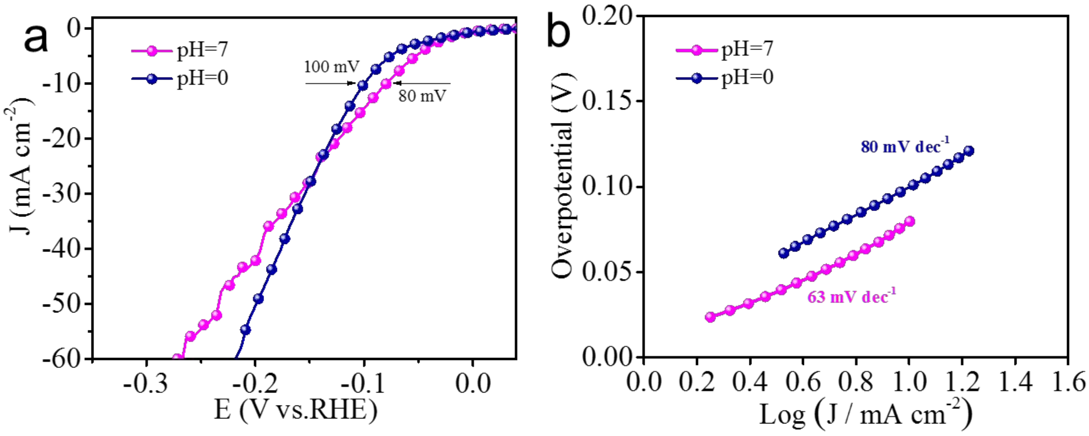

Figure S17. (a) Polarization curves for $Ni_6Mo_6C/NiMoO_x$-400 in pH = 0 and pH = 7 media and (b) corresponding Tafel plot

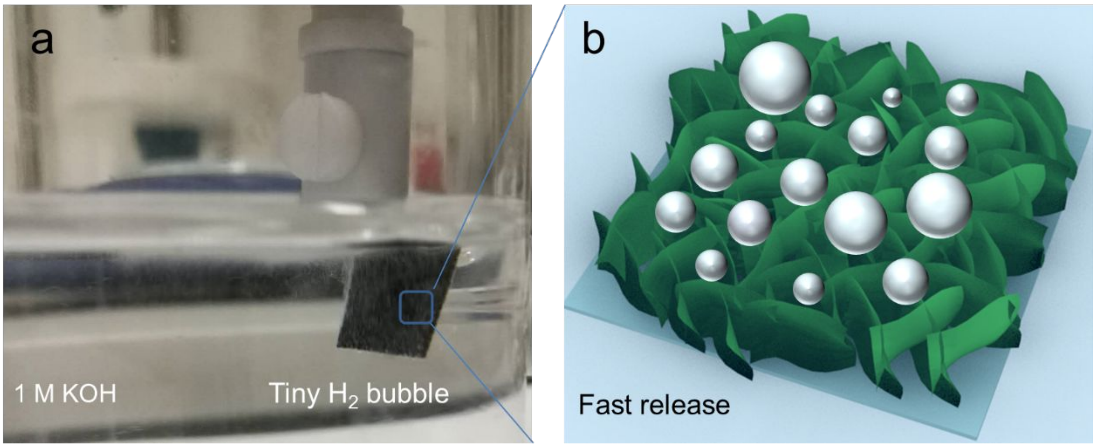

Figure S18. (a) Digital photo of catalyst under electrochemical test (-0.1 V vs. RHE) and (b) schematic illustration of the microstructure of catalyst during HER process.

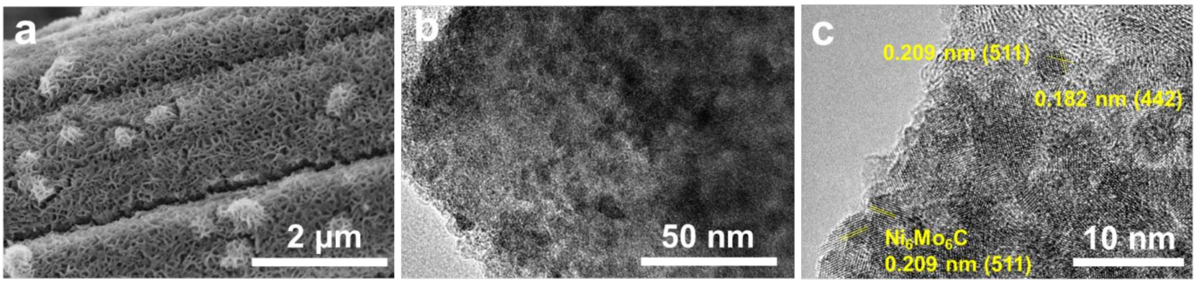

Figure S19. (a) FE-SEM images and (b), (c) HRTEM images of $Ni_6Mo_6C/NiMoO_x$-400 after 60 h i-t test

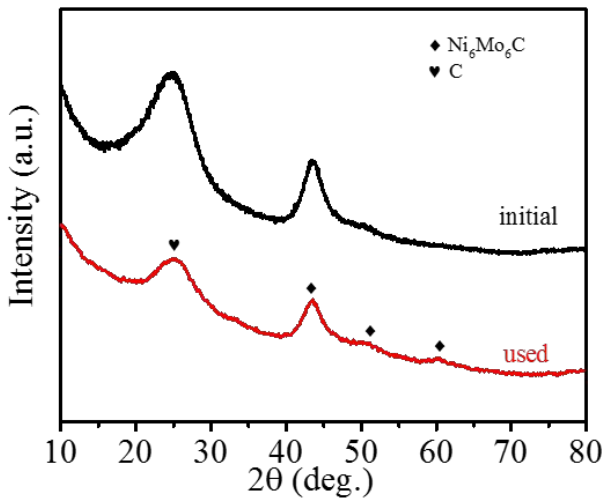

Figure S20. XRD patterns of initial $Ni_6Mo_6C/NiMoO_x$-400 (black) and after i-t test for 60 h in 1 M KOH (red).

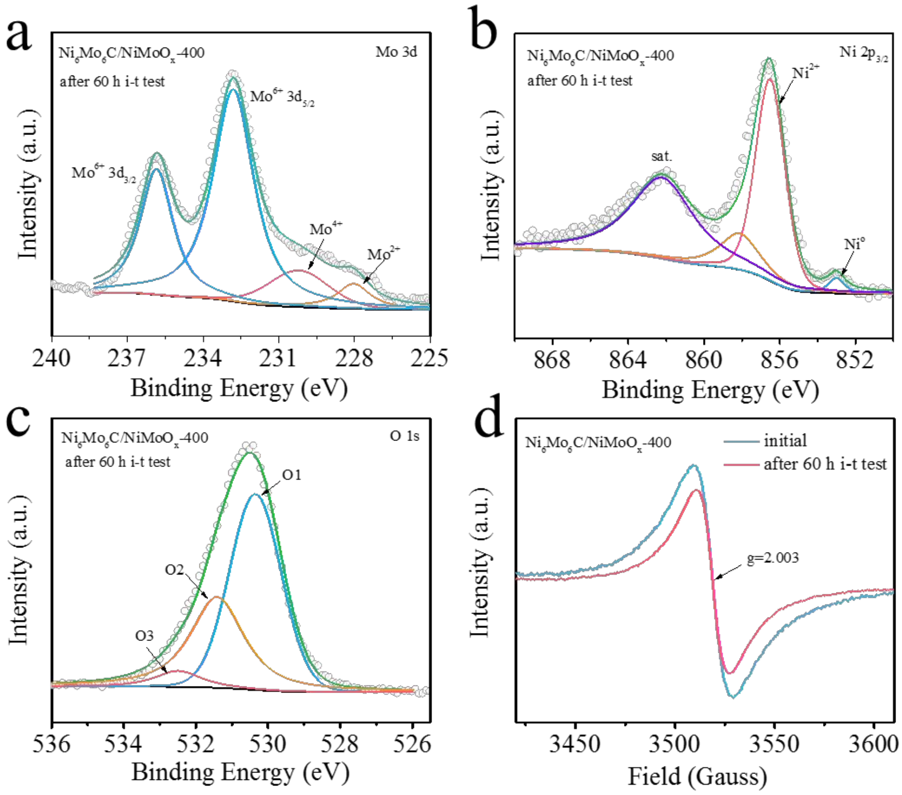

Figure S21. XPS and EPR spectra of $Ni_6Mo_6C/NiMoO_x$-400 after long-term test. High-resolution for the Mo 3d peak (a), Ni $2p_{3/2}$ peak (b), O 1s peak (c) and EPR spectra (d).

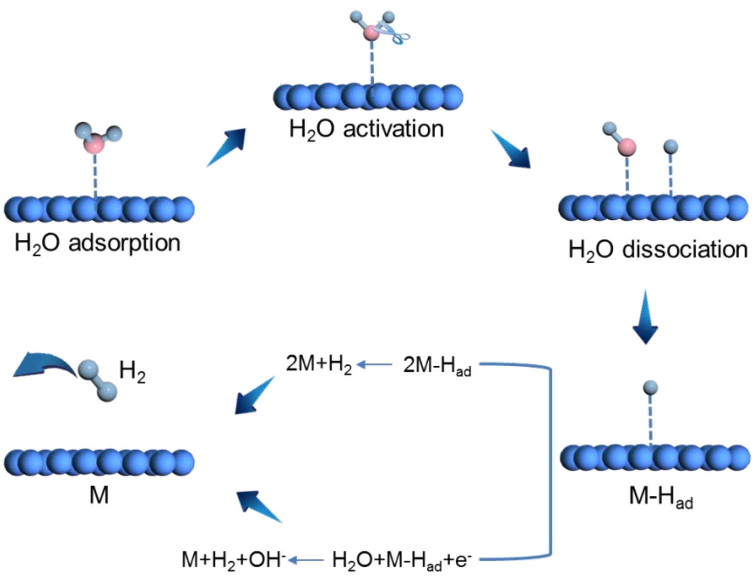

Figure S22. Mechanism of hydrogen evolution reaction under alkaline conditions.

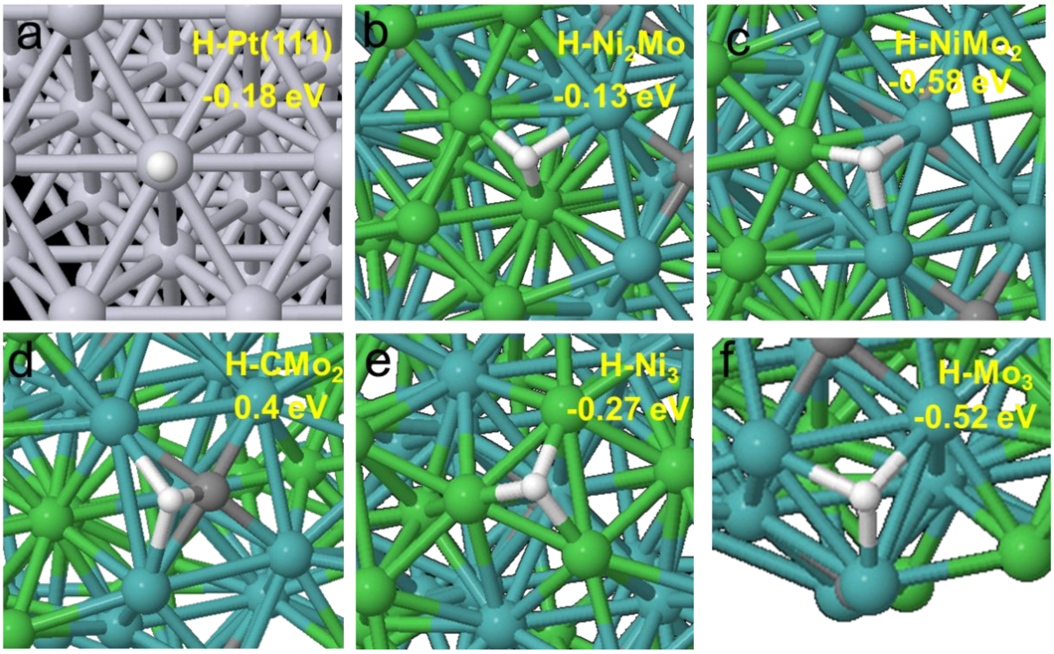

Figure S23. The stable configurations of H adsorption on various sites: (a) Pt (111); (b) Ni_2Mo, (c) $NiMo_2$, (d) CMo_2, (e) Ni_3 and (f) Mo_3 of Ni_6Mo_6C (511). (Ni: green, Mo: cyan, C: black, Pt: grey H: white).

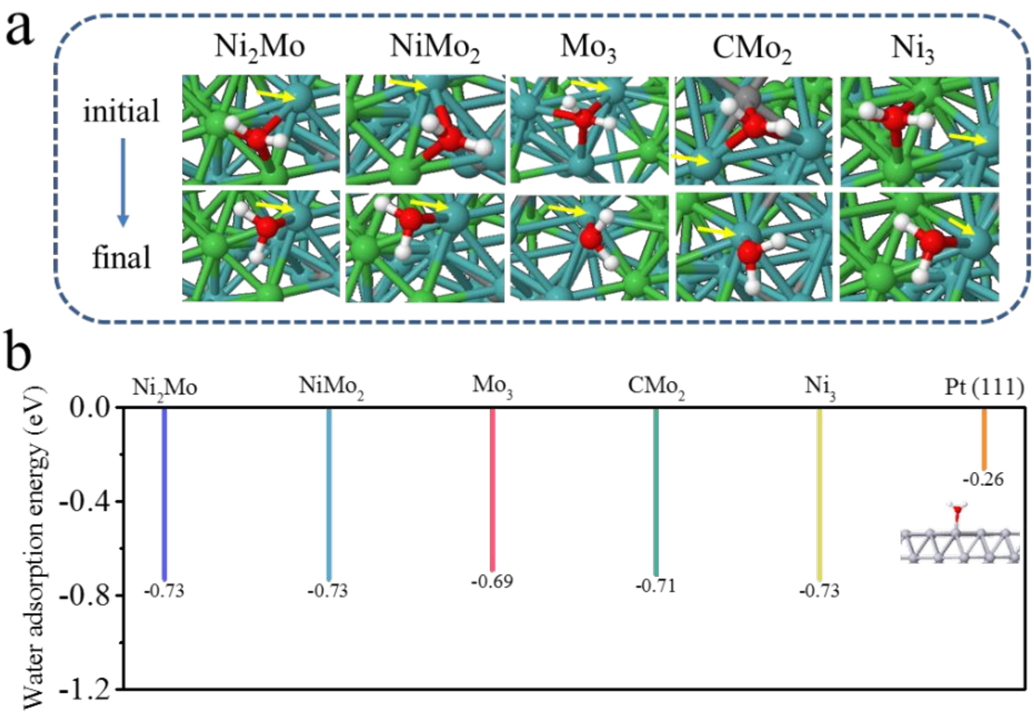

Figure S24. (a) The configurations of initial and final state for water adsorption on different sites of Ni_6Mo_6C (511); (b) Corresponding calculated water adsorption energy of different sites on Ni_6Mo_6C (511) and Pt (111).

Table S1. Comparison of the HER performance for $Ni_6Mo_6C/NiMoO_x$/ACC with other recent transition metal carbides-based catalyst.

Catalysts	η (mV) - j (mA cm^{-2}) Tafer slope (mV dec^{-1}) at lower overpotential regime	Electrolyte	IR compensation	References
$Ni_6Mo_6C/NiMoO_x$/ACC	29-10 42	1 M KOH	×	This work
Mo_2C nanoparticles	176-10 58	1 M KOH	×	1
Mo_2C/G-NCS	70-10 39	1 M KOH	-	2
Mo_2C/2D-NPC	45-10 46	1 M KOH	√	3
Mo_xC@3D N-doped C	122-10 78	1 M KOH	-	4
Mo_2S/Mo_2C	220-1000 43	1 M KOH	√	5
Co-Mo_2C nanowires	118-10 44	1 M KOH	√	6
Mo_xCo_xC@C	83-10 50	1 M KOH	√	7
MoP/Mo_2C@C	75-10 58	1 M KOH	√	8

CoMoC	46-10 46	1 M KOH	-	9
Ni_3Mo_3C/NPC NWS@CC	215-100 106	1 M KOH	√	10
Co-NC@Mo2C	99-10 60	1 M KOH	√	11

Table S2. The surface content of Ni and Mo element of $Ni_6Mo_6C/NiMoO_x$-400 before and after long-term test.

Element \ Catalyst	Initial	After long-term test
Ni (at %)	6.2	6.1
Mo (at %)	3.6	3.3

References

1. Ma, L.; Ting, L. R. L.; Molinari, V.; Giordano, C.; Yeo, B. S. Efficient hydrogen evolution reaction catalyzed by molybdenum carbide and molybdenum nitride nanocatalysts synthesized via the urea glass route. *J. Mater. Chem. A* **2015**, *3*, 8361-8368.

2. Wei, H.; Xi, Q.; Chen, X.; Guo, D.; Ding, F.; Yang, Z.; Wang, S.; Li, J.; Huang, S.; Graphene Nanoarchitectonics: Recent Advances in Graphene-Based Electrocatalysts for Hydrogen Evolution Reaction. *Adv. Sci.* **2018**, *5*, 1700733.

3. Lu, C.; Tranca, D.; Zhang, J.; Rodri Guez Hernandez, F. N.; Su, Y.; Zhuang, X.; Zhang, F.; Seifert, G.; Feng, X. Molybdenum carbide-embedded nitrogen-doped porous carbon nanosheets as electrocatalysts for water splitting in alkaline media. *ACS nano*, **2017**, *11*, 3933-3942.

4. Zhang, H.; Ma, Z.; Liu, G.; Shi, L.; Tang, J.; Pang, H.; Wu, K.; Takei, T.; Zhang, J.; Yamauchi, Y.; Ye, J. Highly active nonprecious metal hydrogen evolution electrocatalyst: ultrafine molybdenum carbide nanoparticles embedded into a 3D nitrogen-implanted carbon matrix. *NPG Asia Mater.* **2016**, *8*, e293.

5. Luo, Y.; Tang, L.; Khan, U.; Yu, Q.; Cheng, H. M.; Zou, X.; Liu, B. Morphology and surface chemistry engineering toward pH-universal catalysts for hydrogen evolution at high current density. *Nat. Commun.* **2019**, *10*, 1-9.

6. Lin, H.; Liu, N.; Shi, Z.; Guo, Y.; Tang, Y.; Gao, Q. Cobalt-Doping in Molybdenum-Carbide Nanowires Toward Efficient Electrocatalytic Hydrogen Evolution. *Adv. Funct. Mater.* **2016**, *26*, 5590-5598.

7. Chen, C.; Wu, A.; Yan, H.; Xiao, Y.; Tian, C.; Fu, H. Trapping $[PMo_{12}O_{40}]^{3-}$ clusters into pre-synthesized ZIF-67 toward Mo_xCo_xC particles confined in uniform carbon polyhedrons for efficient overall water splitting. *Chem. Sci.* **2018**, *9*, 4746-4755.

8. Zhang, L.; Li, S.; Tan, H.; Khan, S.; Ma, Y.; Zang, H.; Wang, Y.; Li, Y. MoP/Mo2C@ C: a new combination of electrocatalysts for highly efficient hydrogen evolution over the entire pH range. *ACS Appl. Mater. Interfaces* **2017**, *9*, 16270-16279.

9. Liu, G.; Bai, H.; Ji, Y.; Wang, L.; Wen, Y.; Lin, H.; Zheng, L.; Li, Y.; Zhang, B.; Peng, H. A highly efficient alkaline HER Co-Mo bimetallic carbide catalyst with an optimized Mo d-orbital electronic state. *J. Mater. Chem. A* **2019**, *7*, 12434-12439.

10. Guo, L.; Wang, J.; Teng, X.; Liu, Y.; He, X.; Chen, Z. A Novel Bimetallic Nickel-Molybdenum Carbide Nanowire Array for Efficient Hydrogen Evolution. *ChemSusChem*, **2018**, *11*, 2717-2723.

11. Liang, Q.; Jin, H.; Wang, Z.; Xiong, Y.; Yuan, S.; Zeng, X.; He, D.; Mu, S. Metal-organic frameworks derived reverse-encapsulation Co-NC@Mo_2C complex for efficient overall water splitting. *Nano Energy*, **2019**, *57*, 746-752.